Current Rectification for Transport of Room-Temperature Ionic Liquids through Conical Nanopores

Xikai Jiang,*,[†] Ying Liu,[‡] and Rui Qiao*,[‡]

[†]Materials Science Division, Argonne National Laboratory, Lemont, Illinois 60439, United States
[‡]Department of Mechanical Engineering, Virginia Tech, Blacksburg, Virginia 24061, United States

ABSTRACT: We studied the transport of room-temperature ionic liquids (RTILs) through charged conical nanopores using a Landau−Ginzburg-type continuum model (Bazant et al. *Phys. Rev. Lett* **2011**, *106*, 046102) that takes steric effect and strong ion−ion correlations into account. When the surface charge is uniform on the pore wall, weak current rectification is observed. When the charge density near the pore base is removed, the ionic current is greatly suppressed under negative bias voltage while nearly unchanged under positive bias voltage, thereby leading to enhanced current rectification. These predictions agree qualitatively with prior experimental observations, and we elucidated them by analyzing the different components of the ionic current and the structural changes of electrical double layers (EDLs) at the pore tip under different bias voltages and surface charge patterns. These analyses reveal that the different modifications of the EDL structure near the pore tip by the positive and negative bias voltages cause the current rectification and the observed dependence on the distribution of surface charge on the pore wall. The fact that the current rectification phenomena are captured qualitatively by the simple model originally developed for describing EDLs at equilibrium conditions suggests that this model may be promising for understanding the ionic transport under nonequilibrium conditions when the EDL structure is strongly perturbed by external fields.
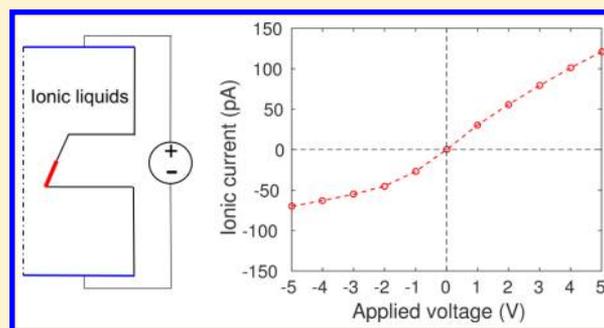
1. INTRODUCTION

Ionic transport in nanopores has numerous applications in biology[1] and electrochemistry.[2] Biological cells communicate with their environment by transporting ions through nanopores in their membrane, which is crucial to metabolism.[3] Electrochemical cells, such as electrochemical capacitors[4] and batteries,[5] rely on the ionic transport between cathode and anode to form a closed circuit to provide power to external circuits.[6] Ions in electrochemical cells are electric current carriers and their transport properties are crucial to cells' performance such as time for charging and discharging.[7,8] Due to its importance in technologies such as nanopore analytics, molecular sensing[9,10] and nanofluidic circuits,[11,12] numerous studies have been conducted to exploit new ionic transport phenomena and physics, and many interesting phenomena have been discovered such as overlimiting current,[13] concentration polarization,[14,15] ion selectivity,[16] ionic enrichment-depletion,[17] anomalous mobility in nanopores,[18,19] ionic current rectification,[20−22] and memory effects for ionic transport through conical nanopores.[23] Recently, ionic current rectification through conical nanopores has been found to regulate charging a capacitor from external fluctuating potential.[24]

Ionic current rectification through nanopores, i.e., the current is different for voltage bias of the same magnitude but different polarity, can be achieved by breaking the symmetry of the nanopores. For cylindrical nanopores, a nonuniform surface charge pattern on the pore wall can lead to rectification;[25] for conical nanopores, uniform and nonuniform surface charge patterns can both lead to rectification.[26] Systematic studies have been done using experiments[27,28] and theories[29−31] to probe the effects of geometry and surface charge on the current rectification. In an earlier experiment,[27] nanopores with tip diameters ranging from 10 to 380 nm were fabricated and their performance was compared. It was found that decreasing nanopore tip diameter, decreasing ionic strength, and increasing surface charge density generally increase the rectification ratio. In a recent experimental work, nanopores with bullet-like tips and lengths of 12 and 23 μm were fabricated, and it was found that increasing pore length increases the rectification ratio.[28] In theoretical studies, a ratchet model was developed: when the nanopore wall is negatively charged, an electrical potential trap will form by applying positive voltages that prevent cation moving toward nanopore tip, in contrast, there is no cation trap by applying negative voltages.[20] An alternative model was developed in which the pore is divided into a region near the tip, a transition region, and a bulk region at the base.[29,30] In this model, the rectification is due to different transference numbers (the fraction of total ionic current carried by a particular ion) in different regions: when cations move from tip to base, they move from a region with higher transference number to a

region with lower transference number, which leads to increasing ion concentration in the pore and a higher conductance; when cations move from base to tip, they move from a region with lower transference number to a region with higher transference number, which leads to decreasing ion concentration in the pore and a lower conductance. Apart from experiments and analytical studies, numerical simulations by solving the Poisson−Nernst−Planck (PNP) equations have been used extensively to study rectification phenomenon. In a pioneering work,[31] a one-dimensional (1D) PNP model was derived in spherical coordinates for long and narrow nanopores with high aspect ratios. This model was shown to quantitatively capture the experimental trends. The 1D PNP model was further extended to describe nanopores tips with conical, bullet-like, trumpet-like, and hybrid shapes, and it was found that the tip shape greatly affects nanopore performances.[32] Using perturbation theory, another 1D PNP model that incorporates entropic effects and charge density renormalization was derived and showed good agreement with experimental data in the regime of small-to-moderate electric currents.[33] More recently, a 1D PNP model that can also consider nanopore with bulk solution reservoirs and allow surface charge density up to −2 e/nm^2 (e is the elementary charge) was developed and it was observed that increasing the length of nanopore increases the rectification ratio.[34] Apart from 1D models, in order to explicitly treat reservoirs with bulk solutions and consider access-resistance[35,36] for shorter pores, 2D axisymmetric PNP models[26,37−39] have been utilized to study rectification and they have showed good agreement with experimental data. Ionic enrichment-depletion in nanopores, which is crucial to changes of nanopore conductance and the rectification, has been observed in the 2D axisymmetric models, and it was found that increasing nanopore length lead to higher rectification ratios. Effects of nonuniform surface charge on nanopore wall on rectification have also been studied and it is found that the thickness and position of transition zone greatly affect the rectification ratios.[26,38]

Most prior studies on the ionic current rectification phenomena focus on dilute electrolytes, while few studies have focused on concentrated electrolytes. As a limiting case of concentrated electrolytes, room-temperature ionic liquids (RTILs) have drawn much attention in recent years. They consist entirely of ions but remain in a liquid state at room temperature and are a promising class of electrolytes due to their remarkable properties such as wide electrochemical window, low vapor pressure, and excellent thermal stability.[40] The interface between RTILs and electrified surfaces plays an important role in the performance of electrochemical devices, for example EDLs at the RTILs−electrode interface greatly affect the capacitance of supercapacitors.[41] Numerous experimental and theoretical studies have revealed intriguing equilibrium properties for EDLs in RTILs, such as alternative layering of ions near electrodes and overscreening.[42−45] Recently, Bazant, Storey and Kornyshev (BSK) developed a Landau−Ginzburg-type continuum model that can capture essential equilibrium properties of RTILs and have yielded good agreement with molecular dynamics (MD) simulations on differential capacitance calculations.[46] For transport properties of RTILs, most prior studies focus on equilibrium transport properties such as self-diffusion of RTILs in nanopores,[47−51] while few studies focus on nonequilibrium transport of RTILs. It has recently been found that EDLs in RTILs can greatly affect transport phenomena in RTILs, and these phenomena

are in sharp contrast with those in dilute electrolytes.[52] From the perspective of ionic current rectifications, Siwy and co-workers[53] performed experimental studies on the transport of RTILs through negatively charged conical nanopores and observed rectification phenomenon. By using a nonuniform surface charge pattern on the pore wall, they achieved large rectification ratios. These observations have been explained qualitatively using arguments similar to that for dilute electrolytes. However, a more thorough understanding of these phenomena, taking into accounting the unique properties of RTILs (e.g., solvent-free), is still missing.

In this paper, we use the BSK model to study the ionic current rectification of RTILs in a negatively charged conical nanopore connected to two reservoirs. Uniform and nonuniform surface charge patterns are studied and compared. Detailed microscopic EDL structures and distributions of ion concentrations, space charge density, and electric field along radial-direction at nanopore tip are analyzed to show how their changes between different bias modes lead to the rectification phenomena and the enhanced rectification when pore wall features nonuniform surface charge patterns.

2. SIMULATION SYSTEM AND MODEL

The simulation system consists of a conical pore connected to two bulk RTIL reservoirs (see Figure 1). The system is
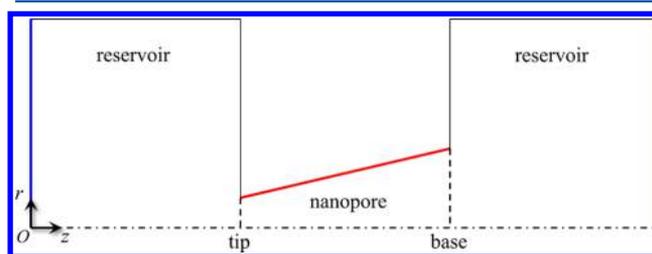

Figure 1. Schematic of the 2D axisymmetric system featuring a conical nanopore and two reservoirs. The pore is connected with bulk reservoirs at the tip and base. Blue lines represent reservoir boundaries where electrical potential is imposed. The reservoir boundary near the pore base is grounded in all simulations. Black and red solid lines represent walls that prevent RTILs penetration. The red line represents the pore wall that carries surface charge density.

modeled in 2D axisymmetric space. The radius of the two openings of the conical pore is 1.5 and 17.6 nm, respectively. The length of the conical pore is 60 nm in the axial direction. The length and radius of both reservoirs are 200 nm. Doubling the length/radius of the reservoir changes the total ionic current by less than 0.1%.

Based on the BSK model developed in ref 46, ionic transport of RTILs through the above system can be described by the following equations:

$$\frac{\partial C_\pm}{\partial t} = D_\pm \nabla \cdot \left(\nabla C_\pm \pm \frac{F}{RT} C_\pm \nabla \phi + \frac{\gamma C_\pm}{1 - \gamma(C_+ + C_-)} \nabla (C_+ + C_-) \right) \tag{1}$$

$$\epsilon_0 \epsilon_{bulk} (l_c^2 \nabla^2 - 1) \nabla^2 \phi = F(C_+ - C_-) \tag{2}$$

where $C_\pm$ is the cation/anion concentration, $D_\pm$ is the ion diffusion coefficient, F is the Faraday constant, R is the ideal gas constant, T is absolute temperature, ϕ is the electrical potential,

γ is the minimum volume available in space for ions, ϵ_0 is the vacuum permittivity, ϵ_{bulk} is the relative permittivity of bulk RTILs, and l_c is the electrostatic correlation length. The ion-free Stern layer is neglected in our system because surface charge density (rather than electrical potential) is imposed directly on the pore walls. The BSK model is parametrized using the properties of the model RTILs.[45] Part of such a parametrization has been performed in ref 46, and the results are as follows: T = 450 K, γ = 0.83 nm^3, l_c = 1.33 nm, and ϵ_{bulk} = 5. With the choice of these parameters, the BSK model can capture overscreening and crowding of EDLs in RTILs, and agrees well with MD simulations of differential capacitance calculations. With these parameters, the diameter of the RTIL ions is ~1.0 nm, the maximal total ion number density that can be achieved in the RTIL is 1.2 nm^{-3}, and the effective thickness of the EDL is 2.0 nm near weakly charged surfaces. In our study, the tip radius of the conical pore is 1.5 nm, so EDL has a weak overlap near the tip of the conical pore. We assume constant diffusion coefficients in the system $D_+ = D_- = 1.0 \times 10^{-11}$ m^2/s, and this value is on the same order of magnitude as those obtained from experimental work on RTILs.[54]

The system of equations, eqs 1 and 2, is closed by the following boundary conditions. On the walls (black and red lines in Figure 1), the ionic flux is zero, and the third derivative of the electrical potential is zero[46] to turn off ion−ion correlation effect. The surface charge density is zero on the reservoir walls (black lines in Figure 1). The dot-dashed line along the z-direction is the symmetry axis of the system. On the reservoir boundaries (blue lines in Figure 1), the ion concentrations are $C_+ = C_- = 0.5$ M = 0.3 nm^{-3}, electrical potentials are applied as Dirichlet boundary condition, and $\frac{\partial^2 \phi}{\partial z^2} = 0$ because the electrical potential varies linearly along the z direction in reservoir at position far away from the nanopore. Both positive and negative bias modes are studied: in the positive (negative) bias mode, a positive (negative) electrical potential is applied on the reservoir boundary near the nanopore's tip (i.e., its narrower opening); the reservoir boundary near the nanopore's base (i.e., its wider opening) is always grounded. The absolute value of total potential drop across the system is varied from 0 to 5 V for both bias modes. Two different patterns of surface charge on the pore wall are studied. In the first one, the pore wall is uniformly charged. In the second one, the left half of the pore wall carries surface charge while the right half of the pore wall is neutral. In both cases, the charged wall has a surface charge density of −0.04 C/m^2. At $t = 0$, $C_+ = C_- = 0.5$ M and $\phi = 0$ throughout the domain. The above equations were solved using a commercial finite element code Comsol.[55] The system was meshed using triangular elements, with the mesh within and near the conical pore heavily refined. The resulting equations were solved using Comsol's time-dependent solver. To ensure convergence, we linearly ramped up the surface charge density to the target value on the pore wall from 0 to 1.68 ms, and then linearly ramped up voltage on the reservoir boundary from zero to target values from 8.4 to 10.08 ms. After that, the system was evolved until a steady state was reached (typically 25.2 ms is enough). The system's mesh was refined several times to ensure that the results are mesh-independent. To validate the calculation results, we computed the distribution of the space charge density normal to the charged pore wall at zero applied voltage. For charged walls in the middle portion of the pore (e.g., z = 230 nm), the distribution of the space charge density normal to

the wall was compared with those reported in ref 46, and excellent agreement was found.

3. RESULTS AND DISCUSSION

3.1. I−V Curves and Current Rectifications. Figure 2 shows the I−V curves for different surface charge patterns.
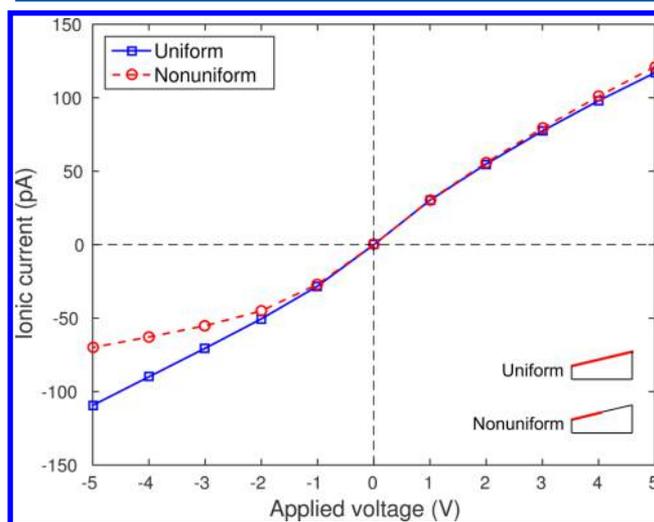

Figure 2. I−V curves for transport of RTILs through conical nanopores with different surface charge patterns.

When the pore wall is uniformly charged, the magnitudes of ionic currents in the positive mode are slightly larger than those in the negative mode, and a maximal rectification ratio of 1.09 is observed at $|V|$ = 5 V. The rectification observed here is weaker than those reported in prior experiments,[53] likely due to the fact that the length of the nanopores is orders of magnitude shorter than that in experiments. Nevertheless, the result confirms that the rectification phenomenon can be reproduced using the BSK model. Given that the BSK model involves only a few parameters, this is quite remarkable. When the pore wall is nonuniformly charged in the positive bias mode, the ionic currents are very close to those for uniform surface charges at the same voltages. In negative mode, the ionic currents are smaller than those for uniform surface charge, and thus the rectification effect is stronger than that obtained for uniform surface charge. A maximal rectification ratio of 1.73 is observed at $|V|$ = 5 V. The enhancement of the current rectification in pores with nonuniform surface charge density is consistent with the experimental observations in ref 53.

In order to understand the rectification phenomenon and the enhanced rectification in conical pores with nonuniform surface charge, we decompose the total ionic current into three components and compare their contributions in different bias modes and surface charge patterns. From eq 1, the ionic current density through the system is

$$j_{tot} = -\left(D \frac{\partial \rho}{\partial z} + \frac{FD}{RT} C \frac{\partial \phi}{\partial z} + \frac{D\gamma\rho}{1-\gamma C} \frac{\partial C}{\partial z} \right) \quad (3)$$

where $C = C_+ + C_-$ is the total ion density, $D = D_+ = D_-$ is the ion diffusion coefficient, and $\rho = C_+ - C_-$ is the ionic space charge density. The first term on the right-hand side of eq 3 is the current contributed by the diffusion of cations and anions. The second term is the current contributed by electrical migration of ions. The third term is the current contributed by

the collective motion of cations and anions driven by the gradient of total ion density, which in turn originates from steric effects. Hereafter, the currents corresponding to these three terms will be denoted by I_{dif}, I_{mig}, and I_{steric}, respectively. While EDL overlapping is not strictly necessary for current rectification, prior experiments[27] did suggest that decreasing tip diameter enhances rectification ratios, so it is worthwhile to analyze the ionic current components and the structure of the EDLs near the tip of the conical nanopore in order to understand the current rectification phenomenon. Here, we chose to perform analysis at the nanopore's tip ($z = 200$ nm in Figure 1). Figure 3 shows the magnitude of the total ionic
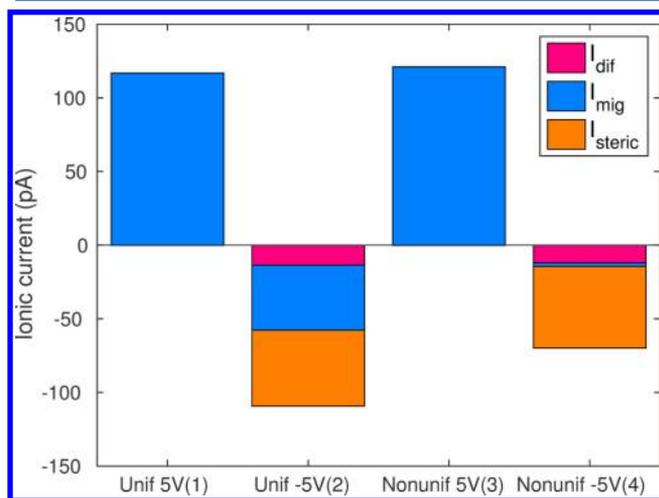

Figure 3. Comparison of total ionic current and its components through the conical pore's tip in four cases characterized by different voltages and surface charge patterns (these cases are denoted by 1, 2, 3, and 4 as indicated on the x-axis).

current and its three components under four different cases characterized by different applied voltages and surface charge distributions. For brevity, these cases are numbered 1 through 4 as indicated on the x axis of Figure 3. In case 1, I_{mig} dominates the total ionic current: I_{dif} and I_{steric} are 2−3 orders of magnitude smaller than I_{mig} and they are practically unnoticeable in Figure 3. In case 2, the three ionic current components are comparable, with I_{dif} being the smallest; I_{mig} is reduced by more than half compared to its value in case 1 and is slightly smaller than I_{steric}. In case 3, I_{mig} still dominates the total current with its magnitude slightly larger than that in case 1, so changing the surface charge pattern from uniform to nonuniform in the positive bias mode does not affect total ionic currents much. In case 4, I_{mig} is significantly reduced compared to case 2, while I_{dif} and I_{steric} only change slightly. From these results, we conclude that it is the significant decrease of I_{mig} that leads to the enhanced current rectification when the surface charge on the pore wall changes from uniform to nonuniform. In the following sections, we perform detailed analyses to show how EDL structural changes lead to rectification in uniform surface charge case and the enhanced rectification in nonuniform surface charge case.

3.2. Current Rectification in Conical Pores with Uniform Surface Charge. To understand what cause the changes in I_{dif}, I_{mig}, and I_{steric} in uniformly charged conical pores when the bias voltage is reversed, we studied the structure of the EDLs and the electric field across the nanopore's tip at ±5 V bias voltages. Figure 4a shows the distribution of the space charge density across the tip of the conical pore. In general, there is a positive space charge layer near the pore wall, and a negative space charge layer is formed next to the positive charge layer. This observation is consistent with the oscillatory space charge distribution of the EDLs in RTILs[56] and lends support to the validity of the BSK model. However, we note that, at a bias voltage of +5 V, there is only a small amount of space charge near the pore wall despite the fact that the wall carries
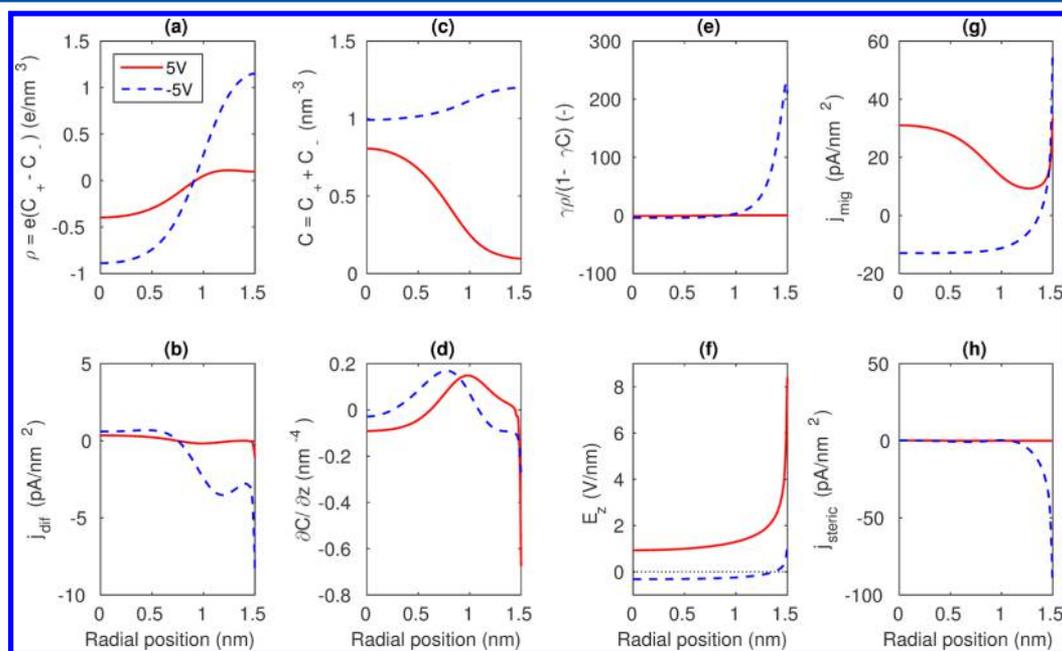

Figure 4. Distribution of various observables across the conical pore's tip ($z = 200$ nm in Figure 1) at +5 and −5 V bias voltages. The pore wall is charged uniformly. (a) ionic space charge density; (b) diffusion current density j_{dif}; (c) total ion density; (d) gradient of total ion density in axial direction; (e) $S = \frac{\gamma\rho}{1 - \gamma C}$; (f) electric field in the axial direction; (g) migration current density j_{mig}; (h) steric current density j_{steric}.

significant negative charges, and the space charge density in the center of the pore is also low. These phenomena are caused by the partial depletion of ions near the pore tip when a positive bias voltage is applied. At + 5 V, cations are pushed toward the nanopore base by the applied electric field; meanwhile, the negative charges on the pore wall repel anions from the wall. As shown in Figure 5a,b, these two effects together create a
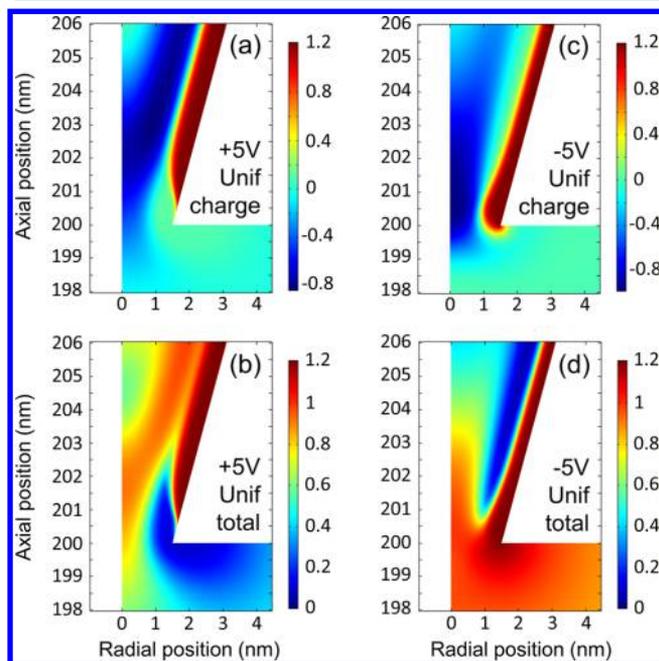

Figure 5. Distribution of ionic space charge density (panels a and c, in unit of e/nm^3) and total ion density (panels b and d, in unit of nm^{-3}) near the tip of the conical pore with different bias voltages. Panels a and b are for +5 V voltage bias, and panels c and d are for −5 V voltage bias.

depletion zone near the pore tip, in which both the space charge density and the total ion density are low. In addition, the region with the strongest space charge density (both positive and negative) is located away from the pore tip to the region between $z = 201$ and 203 nm. Because of these effects, the gradient of the space charge (and hence the diffusion current I_{dif}) is rather small across the pore's tip. At a bias voltage of −5 V, cations are pushed from the pore base to the pore tip by the external electric field. Hence, there is no depletion zone near the pore tip (see Figure 5c,d) and the region with the strongest space charge density is located at the pore tip. Consequently, the gradient of space charge in the axial direction is large at the pore tip (especially a position near the wall), and the resulting diffusion current is much stronger compared to that at +5 V bias (see Figure 4b). Based on the above discussion, we conclude that the much stronger I_{dif} at the pore tip at the negative bias than that at the positive bias is caused by the different response of the EDL structure near pore tip to the externally applied electric field.

We next examine how the migration current I_{mig} varies when the bias voltage is reversed. Since I_{mig} is proportional to the product of total ion density and electric field, these observables will be analyzed first. Figure 4c shows that across the pore's tip, the total ion density is lower at a bias voltage of +5 compared to −5 V, and this is caused by the ion depletion effect described above. As for the electric field in the axial direction E_z, Figure 4f

shows that its magnitude at a positive bias of +5 V is much larger compared to that at a negative bias of −5 V. The stronger field under the positive bias is caused mostly by the ion depletion near the pore tip: because of ion depletion, the negative surface charge on the wall of pore's tip is poorly screened, which strengthens the field due to the imposed positive voltage. This enhancement is especially pronounced near the pore wall. Under a negative bias of −5 V, the incomplete screening of the surface charge on pore walls near the pore tip also leads to a positive electric field. While this electric field is weaker because of the better screening of wall charge compared to that under +5 V bias voltage, it is still strong enough that the net electric field near the pore wall is positive (i.e., opposite to the electric field arising from the externally imposed negative voltage bias). Figure 4g shows the distribution of the migration current density j_{mig} across the conical pore's tip. Overall, j_{mig} is stronger under the bias of +5 V than under the −5 V bias because the axial electric field is stronger under the positive bias. The migration current across the entire pore is in the positive direction under the +5 V bias. Under the −5 V bias, while the migration current in the pore center is in the negative direction (i.e., in the direction of the imposed electric field), the migration current near the pore wall is positive. Because the total migration current is the integral of j_{mig} across the tip ($I_{mig} = \int j_{mig} r \, dr$), and the current near the pore wall contributes more significantly to the total current because of the cylindrical coordinates used in our study, the total migration current under +5 V bias is stronger compared to that under the −5 V bias.

We finally examine the steric current $j_{steric} = -\frac{D\gamma\rho}{1 - \gamma C}\frac{\partial C}{\partial z}$ by analyzing the gradient of the total ion density $\frac{\partial C}{\partial z}$ and $S = \frac{\gamma\rho}{1 - \gamma C}$ (Figure 4e) across the conical pore's tip. While Figure 4d shows that $\frac{\partial C}{\partial z}$ is similar under +5 and −5 V bias voltages, Figure 4e shows that S is much smaller (especially near the wall) at +5 V bias voltage than that at −5 V voltage bias. This is because $1 - \gamma C$, which measures the availability of "voids" in RTILs, is much larger under the positive voltage. As shown in Figure 4c, near the pore tip, ions are locally depleted under +5 V bias but approach close packing at −5 V. Therefore, there are more "voids" in RTILs under the positive bias than under the negative bias; consequently $1 - \gamma C$ is larger. Because $\frac{\partial C}{\partial z}$ is similar under different voltage biases, the steric current is much stronger under negative voltage bias.

Overall, as expected, the electrical migration of ions plays an essential role in determining the ionic current through conical pores. However, under positive voltage bias, the ionic current is dominated solely by the migration current. Under negative voltage bias, the migration current is smaller, and thus the total ionic current is weaker compared to its value under positive bias. However, the migration current under negative bias is compensated by relatively strong diffusion and steric currents. Hence, the net ionic current is only slightly weaker under negative bias than under positive bias, leading to a weak current rectification.

3.3. Enhanced Current Rectification in Conical Pores with Nonuniform Surface Charges. Here we analyze the enhanced current rectification in conical pores with nonuniform surface charges by studying how the patterns of surface charge (uniform vs nonuniform) affect the ionic current under positive and negative biases. Figures 6a−h show that across the tip of
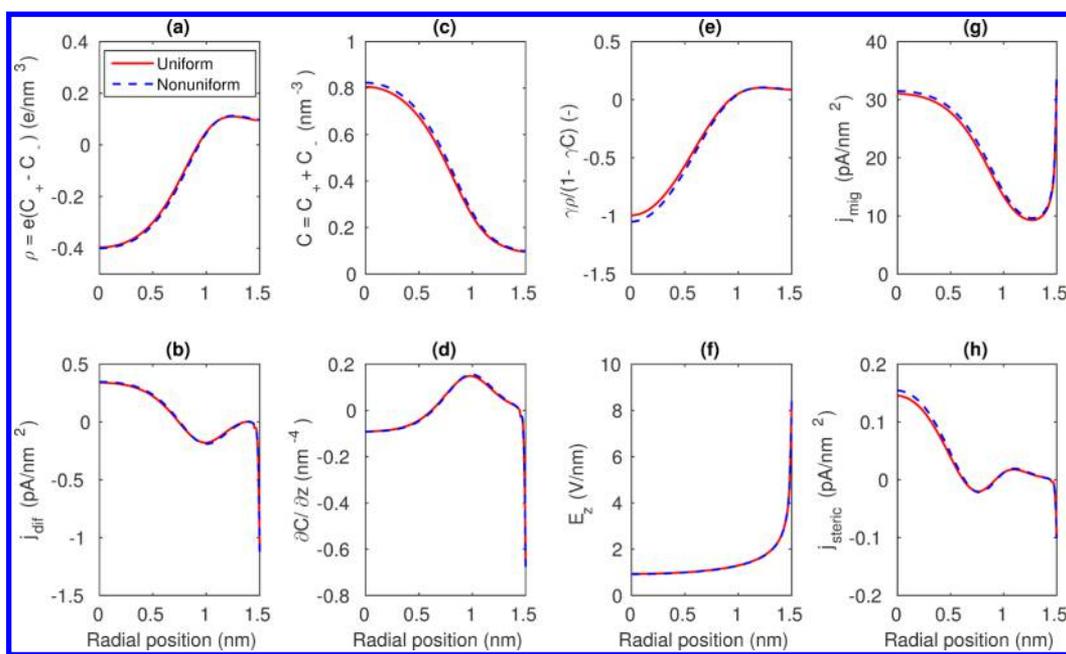
Figure 6. Distributions of various observables across the conical pore's tip at a bias voltage of +5 V when the pore wall is uniformly or nonuniformly charged. (a) ionic space charge density; (b) diffusion current density j_{dif}; (c) total ion density; (d) gradient of total ion density in the axial direction; (e) $S = \frac{\gamma\rho}{1-\gamma C}$; (f) electric field in the axial direction; (g) migration current density j_{mig}; (h) steric current density j_{steric}.
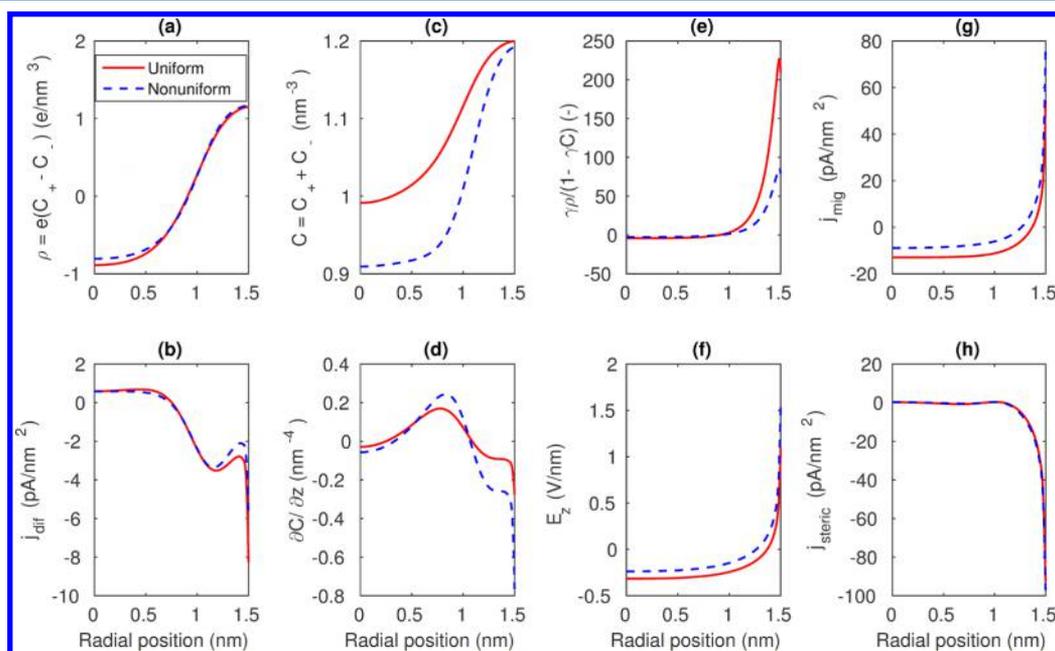

Figure 7. Distributions of various observables across the conical pore's tip at a bias voltage of −5 V when the pore wall is uniformly or nonuniformly charged. (a) ionic space charge density; (b) diffusion current density j_{dif}; (c) total ion density; (d) gradient of total ion density in the axial direction; (e) $S = \frac{\gamma\rho}{1-\gamma C}$; (f) electric field in the axial direction; (g) migration current density j_{mig}; (h) steric current density j_{steric}.

the conical pore, factors affecting the ionic current such as space charge density, total ion density, the axial gradient of total ion density, and the axial electric field exhibit only minute changes when the surface charge pattern changes. The insensitivity of these observables, and thus of the net ionic current, to whether the pore walls near the base of the pore carries negative surface charge or not, is expected. Under positive voltage bias, cations enter the pore tip from the reservoir on its left-hand side, and thus the cation density near the pore tip is only marginally affected by the ion distributions

(and thus by the surface charge) near the pore base. Because cations are the dominating charge carriers near the negatively charged pore tip, it follows that other observables (e.g., anion density) also show little dependence on the surface charge near the base side of the pore.

Figure 7a−h show that, at a bias voltage of −5 V, many factors affecting the ionic transport through pore (e.g., the space charge density) are also only marginally affected by the patterns of the negative surface charge on the pore wall, and the diffusion and steric currents change little. However, the total

ion density and the axial electric field are reduced notably when the negative surface charge on the wall near the pore base is removed (see Figure 7c,f). To understand these observations, we note that under negative bias voltage, cations inside the tip side of the conical pore come from the base side of the pore. When the negative surface charge on that side of the pore is removed, the amount of cations inside the base side of the pore is reduced, and hence the cation density near the tip of the pore is also reduced. The tendency to maintain electroneutrality then forces the anion density to be reduced as well. Consequently, under negative bias voltage, the total ion density is reduced when the negative surface charge on the wall on the base side of the pore is removed. Because of the lower local total ion density, the surface charge on the pore wall is screened less effectively by the RTILs. The axial component of the electric field generated by the surface charge (note that at the pore's tip, this field is in the positive direction) is thus screened less strongly and penetrates more deeply toward the pore center. Consequently, the net axial electric field at the pore tip becomes less negative across the tip. Such a weakened electric field, along with the smaller total ion density, then reduces the migration current greatly, as seen in Figure 3. Because the diffusion and steric current change little (see Figure 7b,h), the total ionic current through the pore is reduced when the negative surface charge on base side of the pore is removed. This, along with the fact that the ionic current at positive bias voltage is affected little by the removal of surface charge near the pore base, leads to a stronger current rectification in conical pore whose wall at its base side is not charged.

4. CONCLUSIONS

In this paper, we used the BSK model to simulate the transport of RTILs in conical pores connected with two reservoirs under bias voltage from −5 to +5 V. Two types of surface charge density patterns have been examined: in the uniform surface charge pattern, the pore wall carries a uniform surface charge density; in the nonuniform surface charge pattern, the left half of the pore wall (adjacent to the narrow pore tip) carries the same surface charge density while the right half of the pore wall is neutral. With the uniform surface charge pattern, the BSK model predicts a weak rectification, with stronger current occurring under positive bias voltage. With the nonuniform surface charge pattern, the current under positive bias voltage changes little while that under negative voltage reduces notably, leading to enhanced current rectification. These observations are in qualitative agreement with previous experimental reports.[53]

The current rectification for the transport of RTILs through conical pores was understood by decomposing the total ionic current through the pore into I_{dif}, I_{mig}, and I_{steric}, and then analyzing the distributions of various factors affect these currents across the conical pore's tip. Under positive bias voltage, there is notable ion depletion near the pore tip. The poorly screened surface charges enhance the electric field driving ionic transport through pore tip, and the net current is dominated by ion migration. Under negative bias voltage, the ion depletion near pore tip is much weaker, but the field arising from the surface charge suppresses the ion migration, leading to a weaker migration current. Because the weaker migration current is partially compensated by the increased diffusion and steric currents (the latter is unique to solvent free electrolytes such as RTILs), only a weak rectification occurs. While removing the negative surface charge on the half of pore wall

near the pore base barely affects the ionic transport under positive bias voltage, it notably weakens the ionic transport under negative bias because ion depletion in nanopore is enhanced when the negative surface charge near the pore base is removed. Overall, the current rectification hinges on the different modification of the EDLs near the pore's tip by the applied voltage biases.

The current rectification in conical pores featuring RTILs and traditional electrolytes share some similarities (e.g., in terms of the observed rectification ratios and dependence on system configuration[20,53]). However, there do exist key differences in their underlying mechanisms. For example, the ionic current due to steric effects, which is important in RTILs but absent in traditional electrolytes, can greatly affect the current rectification. In addition, the solvent-free nature of the RTILs leads to weaker screening of the surface charges on pore wall when ions are depleted near the pore's tip. Such an effect, while much weaker in traditional electrolytes, can greatly affect the electric field and migration current near the pore's tip and hence the current rectification.

The fact that the BSK model can qualitatively capture the current rectification phenomena reported experimentally suggests that the BSK model can be used to study the transport of RTILs under far-from-equilibrium conditions, when the structure of the EDL is strongly modified by external driving forces. Given that the BSK model was developed for predicting the equilibrium properties of EDLs in RTILs, the current findings are encouraging. Our results suggest that the BSK model could be further used to study other geometrical and electrical effects on rectification phenomena. For geometrical effects, the length of the nanopore and the widths of nanopore tip and base can be varied, and cylindrical pores with broken symmetry of surface charge could be studied as current rectification can happen in them as well; for electrostatic effects, magnitude of surface charge densities can be varied. Moreover, the modified Poisson equation in the BSK model has an electrostatic length that can be varied to change the electrostatic strength. There are also approximations used here that can be improved upon. For example, here we assumed that the diffusion coefficients are constants in the whole system. Previous MD simulations showed that the diffusion dynamics of RTILs in cylindrical nanopores with diameters <4 nm can be slower than those in the bulk (see, e.g., ref 51); the diffusion coefficients of RTILs were also showed to be concentration dependent.[57] Hence, rigorously speaking, it is desirable to incorporate such effects into the numerical model, and conceivably the rectification ratio will be modified after these effects are included. However, these effects should not qualitatively affect the rectification phenomenon because the essential mechanisms (e.g., ion depletion and incomplete screening of surface charges near pore's tip) are not affected directly by the variations in ion diffusion coefficient. Future work may explore location/concentration dependent diffusion coefficients in the model to examine their effect on the current rectification.

■ AUTHOR INFORMATION

Corresponding Authors
*E-mail: xikai@anl.gov.
*E-mail: ruiqiao@vt.edu.

Notes

The authors declare no competing financial interest.

REFERENCES

(1) Maret, W., Wedd, A., Eds.; *Binding, Transport and Storage of Metal Ions in Biological Cells*; Royal Society of Chemistry: London, U.K., 2014.

(2) Kontturi, K.; Murtomäki, L.; Manzanares, J. A. *Ionic Transport Processes: in Electrochemistry and Membrane Science*; Oxford University Press: Oxford, U.K., 2008.

(3) Kotyk, A. *Cell Membrane Transport: Principles and Techniques*; Springer Science & Business Media: Berlin, Germany, 2012.

(4) Conway, B. E. *Electrochemical Supercapacitors: Scientific Fundamentals and Technological Applications*; Springer Science & Business Media: Berlin, Germany, 2013.

(5) Yuan, X., Liu, H., Zhang, J., Eds.; *Lithium-Ion Batteries: Advanced Materials and Technologies*; CRC Press: Boca Raton, FL, 2011.

(6) Maier, J. Nanoionics: ion transport and electrochemical storage in confined systems. *Nat. Mater.* **2005**, *4*, 805–815.

(7) Li, N.; Chen, Z.; Ren, W.; Li, F.; Cheng, H. M. Flexible graphene-based lithium ion batteries with ultrafast charge and discharge rates. *Proc. Natl. Acad. Sci. U. S. A.* **2012**, *109*, 17360–17365.

(8) Xu, X.; Yan, M.; Tian, X.; Yang, C.; Shi, M.; Wei, Q.; Xu, L.; Mai, L. In situ investigation of Li and Na ion transport with single nanowire electrochemical devices. *Nano Lett.* **2015**, *15*, 3879–3884.

(9) Howorka, S.; Siwy, Z. Nanopore analytics: sensing of single molecules. *Chem. Soc. Rev.* **2009**, *38*, 2360–2384.

(10) Sha, J.; Hasan, T.; Milana, S.; Bertulli, C.; Bell, N. A.; Privitera, G.; Ni, Z.; Chen, Y.; Bonaccorso, F.; Ferrari, A. C.; et al. Nanotubes complexed with DNA and proteins for resistive-pulse sensing. *ACS Nano* **2013**, *7*, 8857–8869.

(11) Vlassiouk, I.; Siwy, Z. S. Nanofluidic diode. *Nano Lett.* **2007**, *7*, 552–556.

(12) Karnik, R.; Duan, C.; Castelino, K.; Daiguji, H.; Majumdar, A. Rectification of ionic current in a nanofluidic diode. *Nano Lett.* **2007**, *7*, 547–551.

(13) Dydek, E. V.; Zaltzman, B.; Rubinstein, I.; Deng, D. S.; Mani, A.; Bazant, M. Z. Overlimiting current in a microchannel. *Phys. Rev. Lett.* **2011**, *107*, 118301.

(14) Mani, A.; Zangle, T. A.; Santiago, J. G. On the propagation of concentration polarization from microchannel– nanochannel interfaces Part I: analytical model and characteristic analysis. *Langmuir* **2009**, *25*, 3898–3908.

(15) Zangle, T. A.; Mani, A.; Santiago, J. G. On the propagation of concentration polarization from microchannel–nanochannel interfaces Part II: numerical and experimental study. *Langmuir* **2009**, *25*, 3909–3916.

(16) Li, H.; Francisco, J. S.; Zeng, X. C. Unraveling the mechanism of selective ion transport in hydrophobic subnanometer channels. *Proc. Natl. Acad. Sci. U. S. A.* **2015**, *112*, 10851–10856.

(17) Pu, Q.; Yun, J.; Temkin, H.; Liu, S. Ion-enrichment and ion-depletion effect of nanochannel structures. *Nano Lett.* **2004**, *4*, 1099–1103.

(18) Ge, Y.; Xu, D.; Yang, J.; Chen, Y.; Li, D. Ionic current through a nanopore three nanometers in diameter. *Phys. Rev. E* **2009**, *80*, 021918.

(19) Qiu, Y.; Yang, C.; Hinkle, P.; Vlassiouk, I. V.; Siwy, Z. S. Anomalous mobility of highly charged particles in pores. *Anal. Chem.* **2015**, *87*, 8517–8523.

(20) Siwy, Z. S. Ion-current rectification in nanopores and nanotubes with broken symmetry. *Adv. Funct. Mater.* **2006**, *16*, 735–746.

(21) Hou, X.; Liu, Y.; Dong, H.; Yang, F.; Li, L.; Jiang, L. A pH-gating ionic transport nanodevice: asymmetric chemical modification of single nanochannels. *Adv. Mater.* **2010**, *22*, 2440–2443.

(22) Zeng, L.; Yang, Z.; Zhang, H.; Hou, X.; Tian, Y.; Yang, F.; Zhou, J.; Li, L.; Jiang, L. Tunable ionic transport control inside a bio-inspired constructive bi-channel nanofluidic device. *Small* **2014**, *10*, 793–801.

(23) Wang, D.; Kvetny, M.; Liu, J.; Brown, W.; Li, Y.; Wang, G. Transmembrane potential across single conical nanopores and resulting memristive and memcapacitive ion transport. *J. Am. Chem. Soc.* **2012**, *134*, 3651–3654.

(24) Gomez, V.; Ramirez, P.; Cervera, J.; Nasir, S.; Ali, M.; Ensinger, W.; Mafe, S. Charging a capacitor from an external fluctuating potential using a single conical nanopore. *Sci. Rep.* **2015**, *5*, 9501.

(25) Vlassiouk, I.; Smirnov, S.; Siwy, Z. Nanofluidic ionic diodes. Comparison of analytical and numerical solutions. *ACS Nano* **2008**, *2*, 1589–1602.

(26) Qian, S.; Joo, S. W.; Ai, Y.; Cheney, M. A.; Hou, W. Effect of linear surface-charge non-uniformities on the electrokinetic ionic-current rectification in conical nanopores. *J. Colloid Interface Sci.* **2009**, *329*, 376–383.

(27) Kovarik, M. L.; Zhou, K.; Jacobson, S. C. Effect of conical nanopore diameter on ion current rectification. *J. Phys. Chem. B* **2009**, *113*, 15960–15966.

(28) Apel, P. Y.; Blonskaya, I. V.; Orelovitch, O. L.; Ramirez, P.; Sartowska, B. A. Effect of nanopore geometry on ion current rectification. *Nanotechnology* **2011**, *22*, 175302.

(29) Woermann, D. Electrochemical transport properties of a cone-shaped nanopore: high and low electrical conductivity states depending on the sign of an applied electrical potential difference. *Phys. Chem. Chem. Phys.* **2003**, *5*, 1853–1858.

(30) Woermann, D. Electrochemical transport properties of a cone-shaped nanopore: revisited. *Phys. Chem. Chem. Phys.* **2004**, *6*, 3130–3132.

(31) Cervera, J.; Schiedt, B.; Ramirez, P. A Poisson/Nernst-Planck model for ionic transport through synthetic conical nanopores. *Europhys. Lett.* **2005**, *71*, 35.

(32) Ramirez, P.; Apel, P. Y.; Cervera, J.; Mafe, S. Pore structure and function of synthetic nanopores with fixed charges: tip shape and rectification properties. *Nanotechnology* **2008**, *19*, 315707.

(33) Kosinska, I. D.; Goychuk, I.; Kostur, M.; Schmid, G.; Hanggi, P. Rectification in synthetic conical nanopores: a one-dimensional Poisson-Nernst-Planck model. *Phys. Rev. E* **2008**, *77*, 031131.

(34) Pietschmann, J. F.; Wolfram, M. T.; Burger, M.; Trautmann, C.; Nguyen, G.; Pevarnik, M.; Bayer, V.; Siwy, Z. Rectification properties of conically shaped nanopores: consequences of miniaturization. *Phys. Chem. Chem. Phys.* **2013**, *15*, 16917–16926.

(35) Hall, J. E. Access resistance of a small circular pore. *J. Gen. Physiol.* **1975**, *66*, 531–532.

(36) Wang, J.; Ma, J.; Ni, Z.; Zhang, L.; Hu, G. Effects of access resistance on the resistive-pulse caused by translocating of a nanoparticle through a nanopore. *RSC Adv.* **2014**, *4*, 7601–7610.

(37) Liu, Q.; Wang, Y.; Guo, W.; Ji, H.; Xue, J.; Ouyang, Q. Asymmetric properties of ion transport in a charged conical nanopore. *Phys. Rev. E* **2007**, *75*, 051201.

(38) Constantin, D.; Siwy, Z. S. Poisson-Nernst-Planck model of ion current rectification through a nanofluidic diode. *Phys. Rev. E* **2007**, *76*, 041202.

(39) White, H. S.; Bund, A. Ion current rectification at nanopores in glass membranes. *Langmuir* **2008**, *24*, 2212–2218.

(40) Freemantle, M. *An Introduction to Ionic Liquids*; Royal Society of Chemistry: London, U.K., 2010.

(41) Wu, P.; Huang, J.; Meunier, V.; Sumpter, B. G.; Qiao, R. Complex capacitance scaling in ionic liquids-filled nanopores. *ACS Nano* **2011**, *5*, 9044–9051.

(42) Perkin, S. Ionic liquids in confined geometries. *Phys. Chem. Chem. Phys.* **2012**, *14*, 5052–5062.

(43) Hayes, R.; Warr, G. G.; Atkin, R. Structure and nanostructure in ionic liquids. *Chem. Rev.* **2015**, *115*, 6357–6426.

(44) Peñalber, C. Y.; Baker, G. A.; Baldelli, S. Sum frequency generation spectroscopy of imidazolium-based ionic liquids with cyano-functionalized anions at the solid salt−liquid interface. *J. Phys. Chem. B* **2013**, *117*, 5939−5949.

(45) Fedorov, M. V.; Kornyshev, A. A. Towards understanding the structure and capacitance of electrical double layer in ionic liquids. *Electrochim. Acta* **2008**, *53*, 6835−6840.

(46) Bazant, M. Z.; Storey, B. D.; Kornyshev, A. A. Double layer in ionic liquids: overscreening versus crowding. *Phys. Rev. Lett.* **2011**, *106*, 046102.

(47) Singh, R.; Rajput, N. N.; He, X.; Monk, J.; Hung, F. R. Molecular dynamics simulations of the ionic liquid [EMIM+]-[TFMSI−] confined inside rutile (110) slit nanopores. *Phys. Chem. Chem. Phys.* **2013**, *15*, 16090−16103.

(48) Rajput, N. N.; Monk, J.; Hung, F. R. Structure and dynamics of an ionic liquid confined inside a charged slit graphitic nanopore. *J. Phys. Chem. C* **2012**, *116*, 14504−14513.

(49) Rajput, N. N.; Monk, J.; Singh, R.; Hung, F. R. On the influence of pore size and pore loading on structural and dynamical heterogeneities of an ionic liquid confined in a slit nanopore. *J. Phys. Chem. C* **2012**, *116*, 5169−5181.

(50) Singh, R.; Monk, J.; Hung, F. R. Heterogeneity in the dynamics of the ionic liquid [BMIM+][PF6−] confined in a slit nanopore. *J. Phys. Chem. C* **2011**, *115*, 16544−16554.

(51) Singh, R.; Monk, J.; Hung, F. R. A computational study of the behavior of the ionic liquid [BMIM+][PF6−] confined inside multiwalled carbon nanotubes. *J. Phys. Chem. C* **2010**, *114*, 15478−15485.

(52) Jiang, X. Nonequilibrium transport of ionic liquids in electrified nanosystems; Ph.D. Thesis, Clemson University: Clemson, SC, 2015.

(53) Davenport, M.; Rodriguez, A.; Shea, K. J.; Siwy, Z. S. Squeezing ionic liquids through nanopores. *Nano Lett.* **2009**, *9*, 2125−2128.

(54) Noda, A.; Hayamizu, K.; Watanabe, M. Pulsed-gradient spin-echo 1H and 19F NMR ionic diffusion coefficient, viscosity, and ionic conductivity of non-chloroaluminate room-temperature ionic liquids. *J. Phys. Chem. B* **2001**, *105*, 4603−4610.

(55) *COMSOL Multiphysics. User's Guide*, Version 4.3 b, 2014.

(56) Feng, G.; Zhang, J. S.; Qiao, R. Microstructure and capacitance of the electrical double layers at the interface of ionic liquids and planar electrodes. *J. Phys. Chem. C* **2009**, *113*, 4549−4559.

(57) Jiang, X.; Huang, J.; Sumpter, B. G.; Qiao, R. Electro-induced dewetting and concomitant ionic current avalanche in nanopores. *J. Phys. Chem. Lett.* **2013**, *4*, 3120−3126.